From Ab Initio Calculations to Multiscale Design of Si/C Core–Shell Particles for Li-Ion Anodes

ARTICLE *in* NANO LETTERS · MARCH 2014

Impact Factor: 13.59 · DOI: 10.1021/nl500410g · Source: PubMed

3 AUTHORS, INCLUDING:

Maria E. Stournara
Fritz Haber Institute of the Max Planck Society
6 PUBLICATIONS **69** CITATIONS
SEE PROFILE

Yue Qi
Michigan State University
110 PUBLICATIONS **2,494** CITATIONS
SEE PROFILE

NANO LETTERS

Letter

pubs.acs.org/NanoLett

From Ab Initio Calculations to Multiscale Design of Si/C Core–Shell Particles for Li-Ion Anodes

Maria E. Stournara,*[,†] Yue Qi,*[,‡,§] and Vivek B. Shenoy*[,†,∥,⊥]

[†]School of Engineering, Brown University, Providence, Rhode Island 02912, United States

[‡]Department of Chemical Engineering and Materials Science, Michigan State University, East Lansing, Michigan,48824, United States

[§]General Motors Global Research and Development Center, 30500 Mound Road, Warren, Michigan 48090, United States

[∥]Department of Materials Science and Engineering and [⊥]Department of Mechanical Engineering and Applied Mechanics, University of Pennsylvania, Philadelphia, Pennsylvania 19104, United States

Supporting Information

ABSTRACT: The design of novel Si-enhanced nanocomposite electrodes that will successfully mitigate mechanical and chemical degradation is becoming increasingly important for next generation Li-ion batteries. Recently Si/C hollow core–shell nanoparticles were proposed as a promising anode architecture, which can successfully sustain thousands of cycles with high Coulombic efficiency. As the structural integrity and functionality of these heterogeneous Si materials depend on the strength and fracture energy of the active materials, an in-depth understanding of the interface and their intrinsic mechanical properties, such as fracture strength and debonding, becomes critical for the successful design of such and similar composites. Here, we first perform ab initio simulations to calculate these properties for lithiated a-Si/a-C interface structures and combine these results with linear elasticity expressions to model conditions that will avert fracture and debonding in these heterostructures. We find that the a-Si/a-C interface retains good adhesion even at high stages of lithiation. For average lithiated structures, we predict that the strong Si–C bonding averts fracture at the interface; instead, the structure ruptures within lithiated a-Si. From the calculated values and linear elastic fracture mechanics, we then construct a continuum level diagram, which outlines the safe regimes of operation in terms of the core and shell thickness and the state of charge. We believe that this multiscale approach can serve as a foundation for developing quantitative failure models and for subsequent development of flaw-tolerant anode architectures.

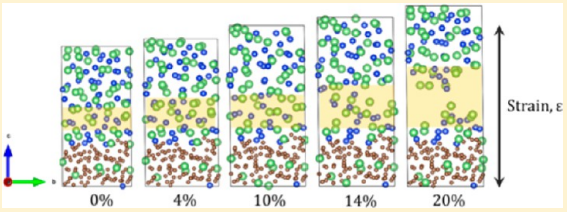

KEYWORDS: *Li-ion battery, Si/C composite anode, ab initio calculations, continuum modeling, Si/C interface strength, fracture*

Silicon is unanimously one of the most attractive and widely investigated candidates for anode materials due to its ultrahigh theoretical specific capacity of 4200 mAh/g, which is 10-fold higher than that of graphite. However, the large volumetric expansion it undergoes during lithium insertion (~300%) is associated with fracture and delamination from the current collector, the active and conductive carbon phase,[1−4] and the surface passivation layer (for example, the solid electrolyte interface (SEI) or protective coatings) between silicon and the liquid electrolyte.[5,6] Hence, it results in rapid capacity fade and loss of cycle life. These modes of failure are attributed to rupture and poor electronic contact of the solid components of the anode (Si/current collector, Si/active phase) at the interface and to the increasing SEI thickness, which fractures during cycling and cyclically forces the electrode-surface to the electrolyte, resulting in continuous consumption of Li^+ respectively.

Clearly, to successfully design next generation high capacity electrodes two critical challenges need to be addressed: the maintenance of good adherence between Si and the conductive phases and the mechanical stability of SEI. To address these issues novel composite nanoengineered structures with increased ratio of surface area over volume have been extensively studied both experimentally and theoretically.[5,7−13]

As recent studies have shown, Si-enhanced nanocomposites with carefully designed interfaces are able to shorten lithium insertion pathways by accommodating for larger strains than the bulk silicon, while maintaining better electronic contacts.[14,15] Excellent examples of such structures are C-based composites in the form of fibers, nanotubes, dendritic structures, powders, polymer binders and others,[11,12,16−18] which combine high capacity and mechanical stability, provided by nanostructured silicon with the high electrical conductivity of carbon.

More recently, Cui et al. and others introduced an electrode architecture that involves Si/C hollow core–shell nanostructures and allows Si electrodes to sustain high capacity over thousands of cycles with high Coulombic efficiency.[6,19−21] This new architecture is of paramount importance for the successful design of next generation Si-enhanced anodes, as it can improve

Received: January 31, 2014
Revised: March 5, 2014

   dx.doi.org/10.1021/nl500410g | *Nano Lett.* XXXX, XXX, XXX–XXX

their mechanical and chemical stability simultaneously. The reason behind this outstanding performance lies in the separation of the electrolyte from the active material (Si) at the inner hollow space: The spherical Si nanoparticle is surrounded by a stiff C-coating, as shown in Figure 1, and this

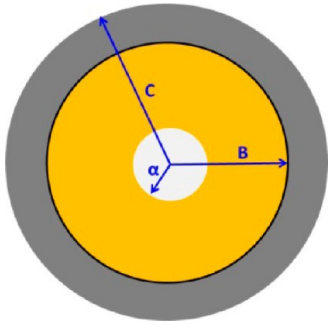

Figure 1. Partially lithiated Si core (yellow) restricted by a rigid C core (gray). The inner radius α accommodates for the deformation of the core.

architecture allows for controlled growth of SEI formation on the C-side. The lithium ions that penetrate through the mechanically rigid shell react with the inner silicon wall, which softens significantly on considerable Li insertion[22,23] and expands inward. Hence, the continuous SEI shedding and reforming is suppressed and as long as the electric contact between the two active materials is maintained, capacity is retained.

Clearly, the successful design of such nanocomposite architectures lies in the structural, mechanical, and electronic properties of the a-Si/a-C interface. Hence, the open question, yet to be addressed, is whether and how lithiation changes the interfacial and fracture strength of these heterostructures. Recently, we used first-principles simulations and calculated more than 20% Li segregation at the interface of lithiated a-Si/Cu structures, in agreement with TOFF-SIMS data, which resulted in significant decrease of the critical shear stress of the interface in agreement with previous experiments.[24] We found that the increasing presence of Li acted as a lubricant for the interface and was responsible for monotonic reduction of the interface sliding strength, τ_{max}, from 0.287 GPa (a-$Li_{0.5}$Si/Cu) to 0.034 GPa (a-$Li_{3.75}$Si/Cu). Our results verified that ab initio simulations, requiring only atomic information as inputs, were excellent in the prediction of structural and mechanical properties of the lithiated amorphous Si/Cu interface by only solving the basic equations of quantum mechanics and statistical mechanics. In contrast to the nonlithiated (111) face-centered cubic (fcc) Cu slab though, the amorphous Si/C interface is highly complicated due to its rough geometry and the fact that Li penetrates both active phases during cycling.

The present letter is aimed (a) to provide a quantitative interpretation of lithiation at the a-Li_xSi/a-$Li_y$$C_6$ structure from ab initio simulations and (b) to combine these results with linear elastic fracture mechanics to model conditions that will avert fracture and debonding in these heterostructures. We show that lithiated a-Si/a-C interfaces adhere well due to strong Si−C bonding, indicating that the two active materials are not threatened by delamination at high stages of lithiation. We then calculate the fracture energy of both active materials and the debonding energy at the interface upon lithiation. Finally, our continuum level analysis reveals the optimum design geometries for the Si/C hollow core−shell structure in terms of the core and shell thickness as a function of the state of charge.

CALCULATION DETAILS

To search for equilibrated a-Li_xSi/a-$Li_y$$C_6$ interfacial structures, we performed ab initio molecular dynamics (AIMD) calculations for both Li_xSi and $Li_y$$C_6$ at finite temperature within the framework of density functional theory (DFT), as implemented in the Vienna ab initio simulation package (VASP).[25,26] The a-Li_xSi bulk configurations were designed as described in ref 24 and the a-$Li_y$$C_6$ compounds were generated from the a-C structure. The latter was simulated by AIMD calculations under the NVT Canonical ensemble with a Nose thermostat at 2000 K for 15 ps and then quenched at 300 K. During quenching, the density/volume of the structure was kept constant. After that, it was allowed to fully relax quantum-mechanically through DFT at 0 K. Starting with an a-C structure with density 3.2 g/cm^3, we constructed each of the lithiated a-$Li_y$$C_6$ configurations by inserting Li atoms one-by-one in the calculated empty Voronoi volumes. Notice that this was not the random mixing approach we took in ref 24 for the design of the a-Li_xSi compounds. The reasons we chose to follow a different lithiation scheme for Li−C system were the following. On the one hand, the host material has a highly dense structure; as more than 75% of the C atoms are sp^3 hybridized at the given density[27,28] the designed a-C structure represents a glassy carbon, whose transition from a random state to an sp^2 configuration is extremely slow even at high temperatures.[29] Therefore, at 3.2 g/cm^3 the a-C structure demonstrated limited empty space, rendering its lithiation by a random mixing lithiation scheme rather difficult. On the other hand, as carbon is much stiffer than silicon it is difficult to simulate lithiation by mixing of Li and C. Therefore, Li insertion had to be done systematically following an iterative process that involved calculation of the larger empty Voronoi volume, addition of one Li atom in the host material and full relaxation at 0 K, until the empty spherical regions were too small to host one extra Li-atom. The numbers of Li, Si, and C atoms corresponding to each concentration used in our calculations are summarized in Table 1.

Starting from the obtained bulk a-$Li_y$$C_6$, three sets of simulation cells were constructed, namely the a-$Li_y$$C_6$ slab, the a-Li_xSi/a-$Li_y$$C_6$ vacuum-interface model, and the a-LiSi/a-$Li_{0.375}$$C_6$ dense-interface model. In the a-$Li_y$$C_6$ slab model,

Table 1. Structural Details of the Interface Structures[a]

bulk amorphous structures	N_{Si}	N_{Li}	N_C	k-points	a-Li_xSi/a-$Li_y$$C_6$ heterostructures	k-points
Si	96			8	Si/C	8
$Li_{0.5}$Si	64	32		36	LiSi/$Li_{0.375}$$C_6$	34
LiSi	48	48		34	$Li_{3.75}$Si/$Li_{0.75}$$C_6$	34
$Li_{1.7}$Si	35	60		20		
$Li_{3.75}$Si	20	75		20		
$Li_{0.125}$$C_6$		2	96	12		
$Li_{0.250}$$C_6$		4	96	12		
$Li_{0.375}$$C_6$		6	96	12		
$Li_{0.750}$$C_6$		12	96	12		
C			96	8		

[a]Number of Li, Si, and Cu atoms corresponding to a-Li_xSi an a-$Li_y$$C_6$ bulk structures and to a-Li_xSi/a-$Li_y$$C_6$ heterostructures, along with the number of irreducible k-points used in the DFT calculations.

dx.doi.org/10.1021/nl500410g | Nano Lett. XXXX, XXX, XXX−XXX

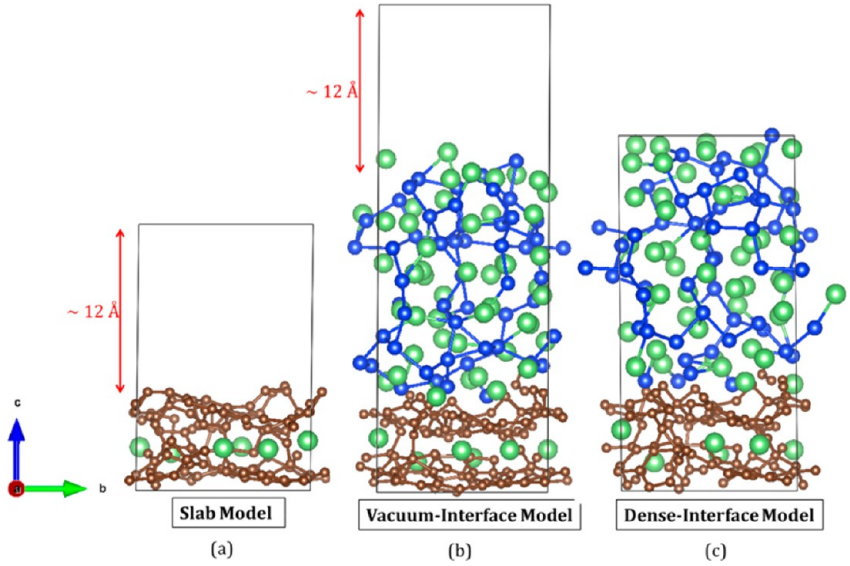

Figure 2. Interface models considered in this study. C atoms are shown as brown, Si atoms as blue, and Li atoms as green spheres.

~12 Å vacuum were added along the *c*-direction in the simulation cell, creating two free surfaces (Figure 2a) and the surface energies of these compounds were calculated as described in Results and Discussion subsection c. In the a-Li_xSi/a-Li_yC_6 vacuum-interface model, the fully relaxed a-Li_xSi bulk configurations were placed on a-Li_yC_6 to form a-Li_xSi/a-Li_yC_6 heterostructures (Figure 2b) and ~12 Å vacuum was added along the *c*-direction to preclude interactions between the a-Li_xSi and the a-Li_yC_6 free surfaces. The atomic positions in both types of models were allowed to relax without changing the cell shape since the atomic layers relaxed into the free space afforded by the vacuum regions above the interface. Finally, the a-LiSi/a-$Li_{0.375}C_6$ dense-interface model was fully periodic consisting of alternating a-LiSi and a-$Li_{0.375}C_6$ layers (Figure 2c). For this dense cell, minimization of both the cell volume and atomic coordinates was required. This model was constructed over a range of cell volumes followed by relaxation of the atomic coordinates in each cell without changing the volume and shape of the cell.

All DFT-based calculations, AIMD, and energy minimization used projector-augmented-wave (PAW) potentials[30] to mimic the ionic cores and the generalized gradient approximation (GGA) in the Perdew–Burke–Ernzerhof (PBE) flavor[31] for the exchange and correlation functional. The plane-wave energy cutoff was 400.0 eV for all the a-Li_yC_6 structures and the a-Li_xSi/Cu interfaces and 500 eV for the diamond calculations based on convergence tests. The convergence tolerance for the electronic relaxation was 10^{-5} eV/cell and the total energy was calculated with the linear tetrahedron method with Blöchl corrections. For bulk a-Li_xSi and a-Li_yC_6 structures, gamma centered 6 × 6 × 6 and 4 × 4 × 4 *k*-meshes were employed respectively, while for the interface a-Li_xSi/a-Li_yC_6 structures, we used a 4 × 4 × 1 *k*-mesh. In addition to the Li_xSi/a-Li_yC_6 heterostructures, we also performed surface calculations of crystalline diamond in order to find the theoretical surface termination phase diagram of Li on C. For bulk diamond, the cohesive energies and bond lengths for different gas molecules were calculated using a 4 × 4 × 4 grid and the irreducible *k*-points in the Brillouin zone used in all calculations are presented in Table 1. All structural relaxations employed conjugate gradient methods to minimize energy of the structure and the required Hellmann–Feynman force[32] on each atom was less than 0.01 eV/Å.

Results and Discussion. To model conditions that will avert fracture and debonding at the a-Li_xSi/a-Li_yC_6 structure, we need to have a quantitative interpretation of lithiation in these heterostructures from ab initio simulations. In the following sections, we present a systematic analysis of the nature of the Si/C interface, along with calculations on the interface adhesion and the fracture energy of the structure. Eventually, we combine the calculated values with linear elastic fracture mechanics to construct a continuum level diagram, which outlines the safe regimes of operation in terms of the core and shell thickness and the state of charge.

a. The Thermodynamic Equilibrium of Li Concentration at Si/C. To simulate lithiation of a core–shell structure at the continuous level with both core and shell being electrochemically active, a typical boundary condition used is to ensure both phases are equilibrated by equating the chemical potentials of the solute (Li) in the two phases, $\mu^{Li}_{Li_xSi} = \mu^{Li}_{Li_yC6}$.[33] Therefore, to build heterostructures that reach thermodynamic equilibrium we considered only equilibrated phases of lithiated Si and C. As the chemical potential for lithium in phase M (M = Si or C), μ^{Li}_{M}, sets the open circuit voltage (OCV) of the system, to design the interface models we first calculated the OCV values corresponding to the different Li_xSi and Li_yC_6 phases. The cell potential for an electrode undergoing a two-phase lithiation reaction is given by Dahn et al.[34] as

$$V = \frac{\Delta G}{\Delta q} = \frac{\Delta E_f + PV - T\Delta S}{\Delta q} \approx -\frac{\Delta E_f}{\Delta x} \quad (1)$$

where V is the electrode potential, ΔG is the difference in free energy between the two phases, and Δq is the charge needed to change the electrode from one phase to the other. If energies are expressed in electronvolts and Δx is the number of lithium atoms transferred, then $\Delta q = -\Delta x$, because there is one electron transferred per lithium *n*. The energy of formation is in the order of several electronvolts, whereas the pressure and entropy terms are two to five times smaller in magnitude, and can therefore be neglected.[35] For a two phase lithiation reaction of M, M = Si, C

dx.doi.org/10.1021/nl500410g | *Nano Lett.* XXXX, XXX, XXX–XXX

$$\mathrm{Li}_x\mathrm{M} + (y - x)\mathrm{Li} \leftrightarrow \mathrm{Li}_y\mathrm{M}$$

the formation energy for $\mathrm{Li}_y\mathrm{M}$ is

$$\Delta E_f = E^{\mathrm{tot}}_{\mathrm{Li}_y\mathrm{M}} - (y - x)E^{\mathrm{tot}}_{\mathrm{Li}} - E^{\mathrm{tot}}_{\mathrm{Li}_x\mathrm{M}} \quad (2)$$

and the average potential versus Li metal is

$$V = E(\mathrm{Li}) - \frac{E(\mathrm{Li}_y\mathrm{M}) - E(\mathrm{Li}_x\mathrm{M})}{y - x} \quad (3)$$

Hence, the average potentials of electrodes in two-phase regions can be obtained by means of total energy DFT calculations. As shown in Figure 3, we calculated the OCV

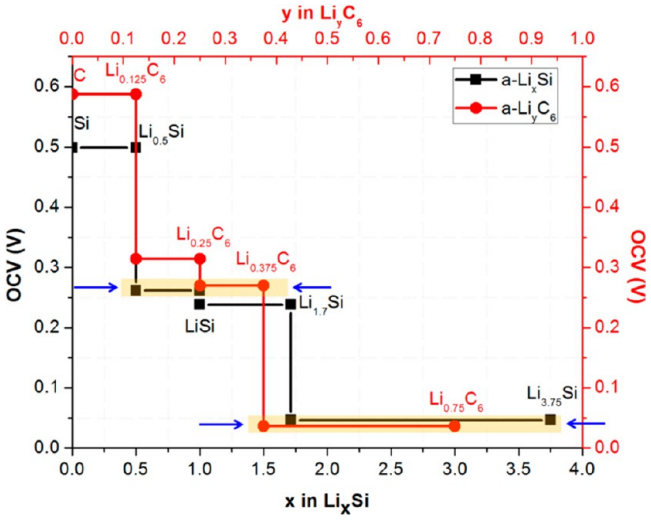

Figure 3. OCV for $\mathrm{Li}_x\mathrm{Si}$ and $\mathrm{Li}_y\mathrm{C}_6$ as a function of Li content. The highlighted regions demonstrated equilibrated Si and C lithiated phases, that is, a-LiSi (a-$\mathrm{Li}_{3.75}\mathrm{Si}$) in equilibrium with a-$\mathrm{Li}_{0.375}\mathrm{C}_6$ (a-$\mathrm{Li}_{0.75}\mathrm{C}_6$).

curves for a-Li_xSi and a-$\mathrm{Li}_y\mathrm{C}_6$ compounds as a function of Li content, which is in good agreement with previous computational and experimental results.[34,36,37] Note that we only used amorphous structures, where the phase transformation upon lithiation is expected to occur smoothly, without sharp phase changes (typical of crystalline systems). To our knowledge the up-to-date reported OCV values for C correspond only to crystalline $\mathrm{Li}_y\mathrm{C}_6$ structures,[37−39] and this is the first study to investigate the voltage profile of amorphous lithiated C compounds. However, this trend, modeled by Chevrier et al. in ref 36, requires numerous intermediate lithiated phases. In this work, we constructed amorphous lithiated Si and C structures based on the predominant lithiated compounds reported in the literature without generating the whole range of possible states of charge. Therefore, in Figure 3 we used straight lines instead of a spline to connect the calculated OCV points corresponding to each lithiated structure. The plateaus also serve as a guide for the eye and identify the equilibrated a-Li_xSi and a-$\mathrm{Li}_y\mathrm{C}_6$ phases used in the interface models. As shown in the highlighted regions, a-LiSi and a-$\mathrm{Li}_{0.375}\mathrm{C}_6$ formed at 0.26 V, while a-$\mathrm{Li}_{3.75}$Si and a-$\mathrm{Li}_{0.75}\mathrm{C}_6$ formed at approximately 0.04 V. These two sets of lithiated compounds served for the design of the a-LiSi/a-$\mathrm{Li}_{0.375}\mathrm{C}_6$ and a-$\mathrm{Li}_{3.75}$Si/a-$\mathrm{Li}_{0.75}\mathrm{C}_6$ equilibrated interfaces, reported in the following sections. We consider that a-LiSi/a-$\mathrm{Li}_{0.375}\mathrm{C}_6$ represents a moderately lithiated interface and a-$\mathrm{Li}_{3.75}$Si/a-$\mathrm{Li}_{0.75}\mathrm{C}_6$ a highly lithiated interface.

b. The Representative Structural Properties of the One Lithiated Si/C Interface. To fully comprehend the properties of the lithiated heterostructures we need to obtain an in-depth understanding of the interface morphology. The critical effect of the Li presence at the interface in the case of the Si/Cu study,[24] underscores the importance of a profound understanding of the structural, mechanical, and electronic properties of the lithiated Si active phase with other conductive materials, such as carbon. In this section we illustrate a detailed study on the moderate lithiated interface, namely a-LiSi/a-$\mathrm{Li}_{0.375}\mathrm{C}_6$, by constructing the two models presented in Figure 4. Both panels demonstrate interface structures, where LiSi was deposited on top of $\mathrm{Li}_{0.375}\mathrm{C}_6$ and relaxed at 0 K, as described in Calculation Details. The difference between the two structures (with the same Li concentrations) lies in the nature of the Li concentration at the interface, as shown in the two highlighted regions: The top panel (Interface I) has Li on the $\mathrm{Li}_{0.375}\mathrm{C}_6$ side located between C atoms, whereas in the bottom panel (Interface II) the $\mathrm{Li}_{0.375}\mathrm{C}_6$ structure has been rearranged so that Li atoms are deposited on top of the C atoms (note that because of the periodicity of the bulk structure, this atomic rearrangement in $\mathrm{Li}_{0.375}\mathrm{C}_6$ did not have any effect on the bulk energy of $\mathrm{Li}_{0.375}\mathrm{C}_6$). We calculated the bottom panel structure to be approximately 8.2 eV higher in energy compared to the top one, indicating that the a-Si/a-C structure is not receptive to excessive Li at the interface; in contrast to the segregation of Li at the Cu surface reported in ref 24, the ample presence of Li at the Si/C interface is unfavorable. This behavior could be attributed to the strong, directional Si−C bonding, which prohibits Li from bonding with C. However, because the interface between the two active materials is amorphous and hence not well-defined, a detailed thermodynamics study of this interfacial zone is a nontrivial task. To systematically investigate the bonding nature of the interface and examine the stability of the interfacial zone, we examined various simpler models of Li- and Si- nonstoichiometrically terminated diamond (111) surfaces. We performed a thorough study of the thermodynamic stability of the various terminations and constructed a contour map (surface phase diagram) by describing the intersection of the various surface energies with the ($\Delta\mu_{\mathrm{Li}}$, $\Delta\mu_{\mathrm{Si}}$) chemical potential plane. Our results suggested that the Si-terminated surfaces were stable in a much larger phase space than the Li-terminated ones and that at surface exposure to Li and Si the termination would be predominantly Si (by 75%-see Supporting Information). This finding further explains why Interface I is more energetically favorable and suggests that Li segregation at the Si/C interface is an unlike event.

To explore the bonding character of the two interface models, we mapped their electron density distributions with the use of the electron localized function (ELF),[40] a position dependent function with values that range from 0 to 1; ELF = 1 corresponds to localization (i.e., a covalent bond), and ELF = 0.5 corresponds to electron-gaslike pair probability (i.e., a metallic bond), whereas for values less than 0.5, it is undefined. As shown in Figure 4a, Interface I demonstrates ELF ≈ 0.8−0.9 with a well-localized charge density along the Si−C bond (projected with orange color on the *xy*-plane), and the calculated average Si−C bond length at 1.90 Å. On the contrary, Interface II (Figure 4b) shows a much more diffused profile (green color) with ELF ≈ 0.5 and Li−C = 2.52 Å, indicating the metallic character of the interface.

Bader charge analysis was used to partition electrons and atoms, where the atomic volumes and charges were determined

dx.doi.org/10.1021/nl500410g | *Nano Lett.* XXXX, XXX, XXX−XXX

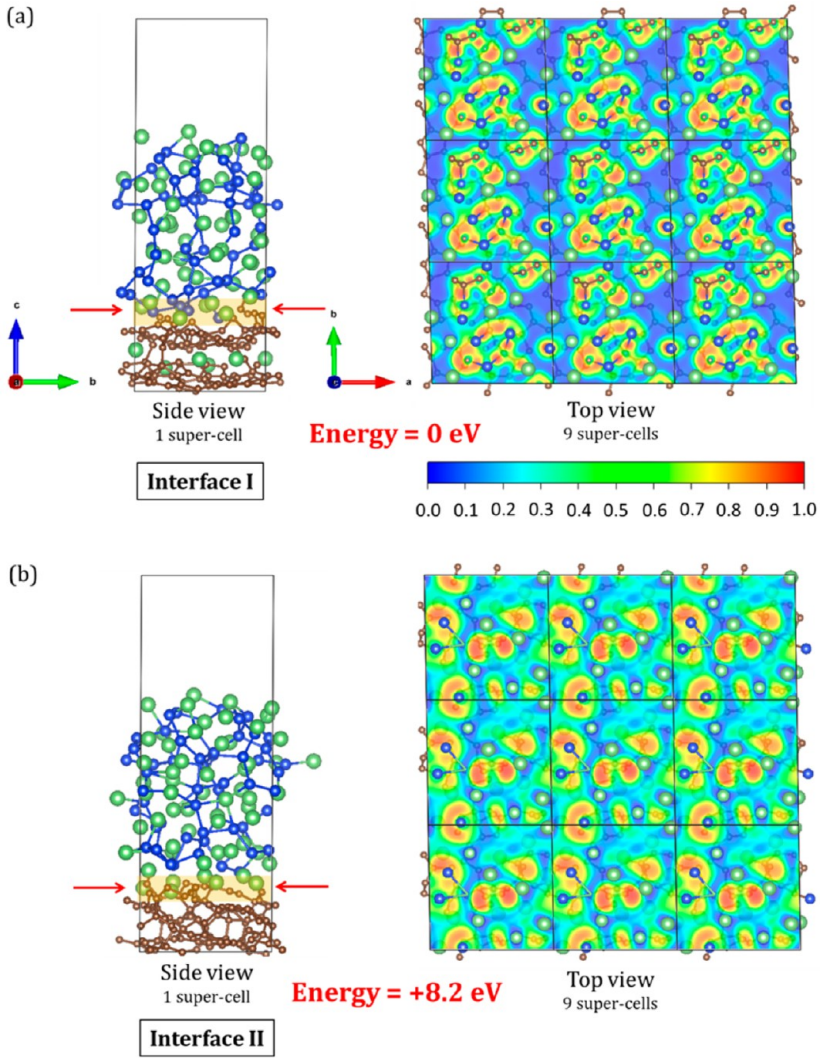

Figure 4. Side and top view of two a-LiSi/a-$Li_{0.375}C_6$ vacuum-interface models. In (a), Li atoms on the C-side are located between C atoms and the interface is terminated by both Si and Li, giving rise to strong ionic Si−C bonding. In (b), Li atoms are on top of the C atoms, as a way to simulate Li segregation at the interface and the interface is primarily dominated by Li atoms. The diffuse metallic character of Li−C bonding is predominant. For both models, the ELF contour plots were calculated at 6.2 Å (surface pointed by the red arrows in the highlighted region).

Table 2. Bader Charge Analysis of the Two a-LiSi/a-$Li_{0.375}C_6$ Interfaces[a]

model	NLi_{surf}	NSi_{surf}	NC_{below}	Li	Si	C below Li and Si	bulk C
interface I	5	5	10	4.498	4.588	−9.084	−0.008
interface II	5	5	10	5.007	−0.667	−5.682	0.006

[a]Values show the total amount of charge transferred with a positive value representing charge accumulation and a negative value the charge depletion on the corresponding atom.

according to the charge density distribution.[41] The net charges on Li and Si appear in Table 2. The C atoms at the center of the amorphous slabs were almost neutral ($e^- < 0.008$) for both models, whereas the charges on Li and Si interface atoms are different depending on the structure. In Figure 4a, where the interface is populated by both Li and Si atoms, the topmost C atoms received in total −9.084 electrons from the approximately equal charge contributions of both Li and Si. However, upon Li segregation at the interface (Figure 4b), only Li provided charges to the topmost C atoms, which received in total only −5.682 electrons. This significant decrease in the charge transfer at the presence of excessive Li resulted in weaker electrochemical interaction between the two active materials and was reflected in the 8.2 eV increase in energy. This finding is in excellent agreement with prior work reported by Sen et al.,[42] where they suggested that the interface bond strength was found to increase with the charge density of the adatoms and the amount of charge transfer. In particular, they showed that

$$W_{sep} \propto \frac{(n_{WS} + \Delta Z)}{d^2} \tag{4}$$

where the numerator on the right-hand side indicates the interatomic density at the boundary of the Wigner−Seitz cell of the interface, n_{WS}, enhanced by the charge transfer between interfaces, ΔZ, and the denominator, d, is the bond distance

dx.doi.org/10.1021/nl500410g | Nano Lett. XXXX, XXX, XXX−XXX

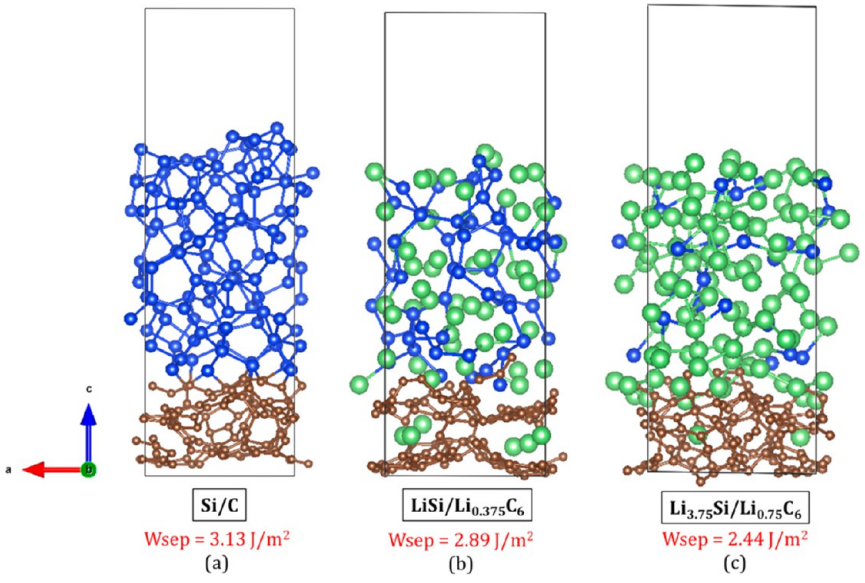

Figure 5. W_{sep} for vacuum-interface models of equilibrated lithiated Si/C. The interface retains good adherence even at high stages of lithiation (~20% reduction in W_{sep}).

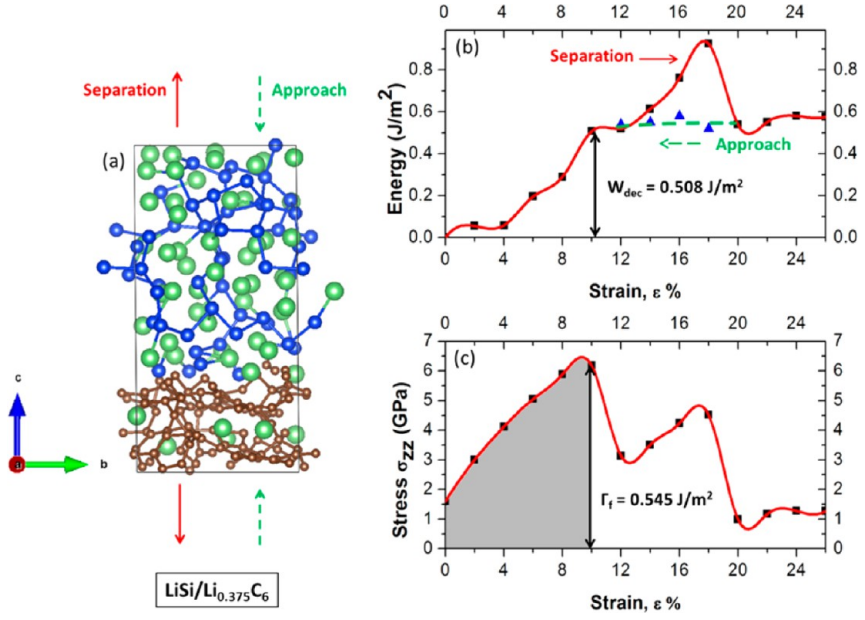

Figure 6. (a) The dense-interface model of a-LiSi.a-$Li_{0.375}C_6$, (b) energy per area (J/m^2)m and (c) stress (GPa) as a function of strain along the *c*-direction.

between the different materials at the interface. By comparison to the Si/Cu interface in ref 24 and the Si/graphene interface in ref 43 where the metal current collector is only an electron, yet not a Li-ion receptor, the amorphous C in Si/C takes both the +1 electron and the Li-ion itself. Hence, the latter interface demonstrates stronger chemical bonding interaction (covalent Si−C bonds) between the two active materials, whereas in the former case the interface adhesion is due to pure electrostatic interaction.

c. Interface Strength of the a-Li_xSi/a-Li_yC_6 at Different Li Concentration. To evaluate the debonding energy Γ_d of the lithiated Si/C interface, we calculated the work of separation at the interface of the a-Li_xSi/a-Li_yC_6 heterostructures. The standard definition of W_{sep} is

$$W_{sep} = \sigma_1 + \sigma_2 - \gamma_{12} = \frac{E_1^{tot} + E_2^{tot} - E_{12}^{tot}}{A} \quad (5)$$

where σ_i is the surface energy of the slab *i*, γ_{12} is the interface energy, E_i^{tot} is the total energy *o*f slab *i*, E_{12}^{tot} is the total energy of the interface system with slab materials 1 and 2, and *A* represents the total interface area.[44] This is the energy required to break bonds at the interface to completely separate along the interface normal. We used the a-Li_xSi/a-Li_yC_6 vacuum-interface model to calculate W_{sep} as a function of the Li concentration (Figure 5). As the Li content increased in Li_xSi (Li_yC_6) from x = 0 (y = 0) to x = 3.75 (y = 0.75), separating the interface required less energy and W_{sep} decreased. As shown in Figure 5, the reduction of W_{sep} by approximately 20% (W_{sep} reduces from 3.13 to 2.44 J/m^2) indicates only slight interface weakening,

dx.doi.org/10.1021/nl500410g | Nano Lett. XXXX, XXX, XXX−XXX

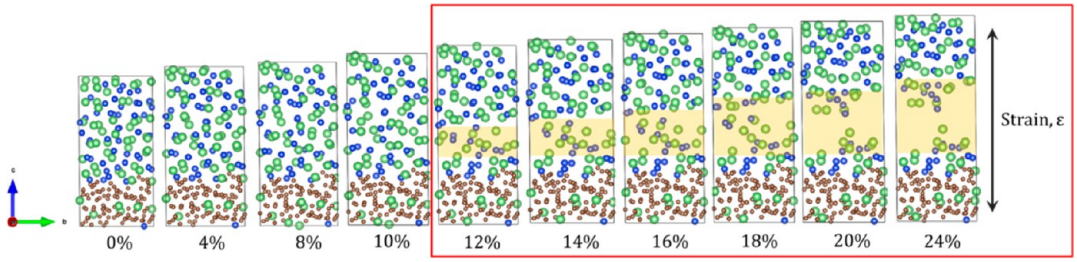

Figure 7. Fully relaxed structures at various stages of strain along the *c*-axis. The yellow highlighted regions demonstrate the locus of fracture. The structure ruptures at ε = 12% and bond break and reform occurs until ε = 18%. After ε = 12%, the structure is completely fragmented.

which suggests relatively good adhesion between the two active materials, even at high states of charge.

Evaluating the interface mechanical property of the a-Li_xSi/a-Li_yC_6 vacuum-interface model contributed to our understanding on the interfacial bonding nature of the lithiated Si/C hollow core−shell particle. However, to comprehend fracture in the structure we need the fracture energy, Γ_f. For an average lithiated structure, fracture was simulated with the application of tensile strain along the *c*-axis of the a-LiSi/a-$Li_{0.375}C_6$ dense-interface model as show in Figure 6. Starting with the minimum-energy structure as the reference state (0% strain state), the interface couples were uniformly elongated at a 2% strain increment, followed by minimization of all atoms to obtain the relaxed geometries. In this process the interface model shall fracture at its "weakest link", which is not necessarily at the interface. The strain was then incremented and the process continued up to fracture. As the cell was monoclinic with α, β, and γ angles approximately, but not exactly 90°, the application of strain along the *c*-direction (a_{zz} element of the first lattice vector) slightly modified the a_{yz} and a_{xz} matrix elements of the other two lattice vectors. Therefore, the cell lengths along the *x*- and *y*- directions are not kept fixed, but they undergo infinitesimal increments in the order of 0.003 to 0.1 GPa upon every strain increase.

The work of decohesion, W_{dec} (equivalent to the fracture energy due to bond rupture, Γ_f) is defined as the energy difference (per unit surface area) between the fractured system and the interface structure at a zero stress state.[44] As shown in Figure 6, W_{dec} was computed to be 0.508 J/m^2. That is more than five times smaller than the calculated work of separation at the interface (W_{sep} = 2.894 J/m^2), suggesting it is more energetically favorable for the system to fracture within the Li_xSi slab than at the interface. This finding was further verified by calculation of the fracture energy Γ_f as the integral of the stress−strain curve up to the fracture point, which gave 0.545 J/m^2, in very close agreement with the decohesion energy given by the energy calculations. The energy barrier during the separation of the two interfaces, which was about 0.40 J/m^2, is caused by metastable structures formed during separation. As shown in the curve (Figure 6), when the two free surfaces approach each other in the reverse process the barrier is significantly reduced. The calculated fracture strength was 6.18 GPa, which is in excellent agreement with previous experimental studies.[45,46] This finding was further supported by calculating the Li−Li, Li−Si, and Si−Si bond lengths in the strained and unstrained structures. Employing the radial pair distribution function $g(r)$ at 1200 K, we computed the first neighbor in the relaxed unstrained structure to be: Li−Li ∼ 3.1 Å, Li−Si ∼ 3.05 Å, and Si−Si ∼ 2.8. As shown in Figure 7, application of strain along the *c*-axis results in fracture within the lithiated Si slab. In particular, fracture occurs at ε = 12%, where the average bond distance between Li−Li, Li−Si, and Si−Si at the locus of fracture (highlighted in yellow) was in the order of 3.3, 3.15, and 3.1 Å accordingly. Until ε = 18%, various metastable structures involving bond rupture and reform are generated, and for ε > 18% the structure is completely fragmented.

Finally, to understand fracture of the carbon coating due to the tensile stress during lithiation, we evaluated the a-C fracture energy by computing the surface energies of a-Li_yC_6 slab model. The standard definition of the surface energy of the slab σ_i is

$$\sigma_i = \frac{E_i^{slab} - E_i^{bulk}}{2A} \quad (6)$$

As expected, the surface energy of a-Li_yC_6 compounds was significantly higher compared to the one of a-Li_xSi compounds. In particular, the calculated values for a-C, a-$Li_{0.375}C_6$, and a-$Li_{0.75}C_6$ were 9.28, 9.12, and 8.96 J/m^2 accordingly. To verify this finding, we also computed the surface energy of diamond (111) surface, which was found to be 11.42 J/m^2, in close agreement with Field at al.[47] Because the amorphous structure is less ordered than diamond, the C−C bonding in a-C is distorted; not all C atoms are sp^3 hybridized and therefore, the surface energy of a-C (9.28 J/m^2) is lower than that for diamond. The computed values for the surface energies are not significantly affected by the presence of Li, suggesting that in contrast to the bond softening occurring in the bulk and surface of Li_xSi the strong covalent C−C bond in Li_yC_6 does not change its character upon lithiation.

d. Fracture and Debonding in the Lithiated Hollow Si/C Core−Shell Particle. Ab initio simulations, requiring only atomic information as inputs, are excellent in the prediction of basic material properties by solving the basic equations of quantum mechanics and statistical mechanics. To model fracture and debonding at the continuum level we used the calculated values from the a-Li_xSi/a-Li_yC_6 DFT analysis described in previous sections.

To successfully design hollow core−shell architectures, we need to accommodate for (a) the compressive and tensile hoop stresses that the core and the shell undergo respectively during lithiation with the latter being responsible for fracture of the shell and for (b) the radial tensile stress in both the core and the shell during delithiation. In ref 48, Zhao et al. provide a thorough fracture and debonding analysis on Si/Al_2O_3 hollow spherical particles, where they assume that delamination occurs at the Si/Al_2O_3 interface and estimate Γ_d = 1 J/m^2. Here, we use this approach to analyze fracture and debonding in Si/C nanoparticles. However, instead of assuming that delamination occurs at the interface, we use the DFT calculated values, which demonstrate that debonding occurs within the lithiated Li_xSi

dx.doi.org/10.1021/nl500410g | *Nano Lett.* XXXX, XXX, XXX−XXX

slab and not at the interface, as discussed in Results and Discussion subsections b and c. Hence, an essential first step toward an in-depth understanding of the role of lithiation on hollow core−shell Si/C nanoparticles is achieved by employing our ab initio results from the atomic level analysis of Si/C slabs as useful input parameters for the continuum level analysis of the Si/C nanoparticle.

The geometric relation that should be satisfied to completely fill the hollow space upon lithiation is defined in ref 48 as

$$\mathrm{SOC}_{\mathrm{full.lithiation}} = \frac{A}{B} = \left(\frac{\beta - 1}{\beta}\right)^{1/3} = \left(\frac{3}{4}\right)^{1/3} \tag{7}$$

where the volumetric swelling ratio $\beta = V_f/V_i$, with V_f representing the fully lithiated volume and V_i the initial volume of the lithium-free state. Lithiation of silicon causes a volumetric swelling $\beta = 4$. At a given state, the state of charge (SOC) is calculated by using the inner radius α (Figure 1)

$$\mathrm{SOC} = \frac{A^3 - a^3}{A^3} \tag{8}$$

Combining eqs 7 and 8, we can define the inner radius α as a function of the SOC

$$a = B\mathrm{SOC}_{\mathrm{full\_lithiation}}(1 - \mathrm{SOC})^{1/3} \tag{9}$$

From linear elastic fracture mechanics, the simplified expression for the energy release rate during fracture of the coating due to the tensile hoop stress in the shell is

$$G_f = 2\frac{\sigma_Y^2}{E_s}\left(\log\frac{B}{\alpha}\right)^2 \frac{B^2}{C - B} \tag{10}$$

where E_s is the Young's modulus of the Si shell, σ_Y the yield strength of Si and α, B, and C are the inner, core, and particle radius, respectively, presented in Figure 1. Likewise, the energy release rate due to debonding, as a result of the tensile radial stress of the lithiated Si/C shell is

$$G_d = 4\pi\frac{\sigma_Y^2}{E_e}\left(\log\frac{B}{\alpha}\right)^2 (C - B) \tag{11}$$

The critical conditions for fracture of the shell and debonding within the Li_xSi core are $G_f = \sigma_C$ and $G_d = W_{dec}$, respectively. Therefore, applying the calculated debonding energy of a-$Li_{3.75}Si$/a-$Li_{0.75}C_6$ $W_{dec} = 0.545$ J/m^2 and the fracture energy of a-C the coating, $G_f = 9.28$ J/m^2 reported in Results and Discussion subsection c in eqs 10 and 11, we constructed diagrams that indicated the optimum range of dimensions for core and shell as a function of the SOC. We used representative values of lithiated silicon and carbon: $\sigma_Y^{Li} = 1$ GPa,[49] $E_C = 12$ GPa[22] for lithiated Si and $\sigma_Y^C = 1220$ GPa for C.[50] Following Zhao's approach,[48] we plotted the conditions for fracture and debonding of a hollow Si/C core−shell structure as a function of the SOC (Figure 8). Note that to represent the change from pure Si to pure Li in this and the following sections, we define concentration y for a-Li_xSi, via the expression $\mathrm{SOC} = x/(1 + x)$. Hence, while x is the atomic ratio of Li/Si, y is the ratio of the Li atoms to the total number of atoms. The advantage of using SOC in favor of x is that for elemental Li $x \to \infty$, while y is 1. Therefore, all the compounds can be explored by letting SOC vary between 0 (Si) and 1 (Li). The safe regimes lay in the gray shaded areas bounded by the critical conditions for fracture (blue line) and debonding (red line). Using the experimental

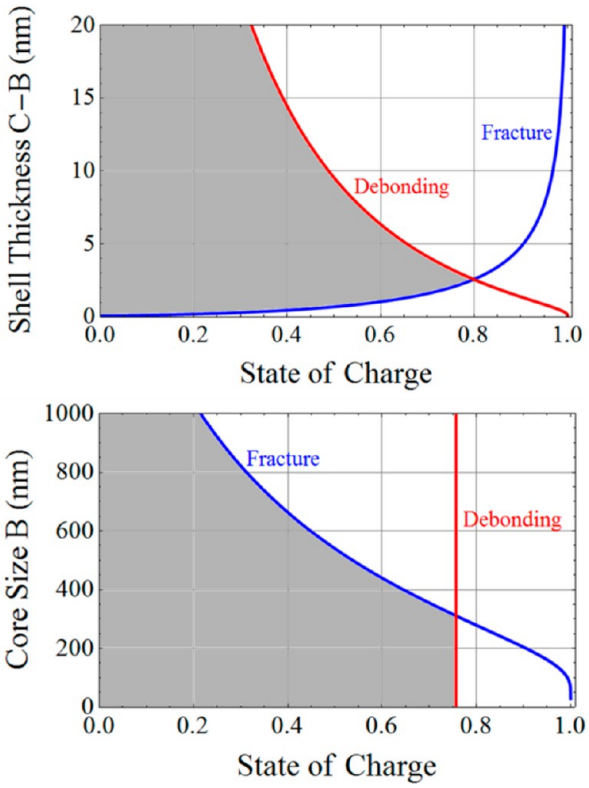

Figure 8. Conditions of fracture and debonding, according to the formulation derived by Zhao et al.[48] and the DFT computed values for the decohesion energy, W_{dec} from this work. The shaded regions demonstrate the safe regimes of operation as a function of top shell thickness and bottom core size with state of charge.

value for the particle's shell thickness, we defined it to be $C - B$ = 20 nm thick[20,21] and mapped the safe operation regime with SOC by varying the core thickness. Similarly, we assumed core thickness $C = 200$ nm and varied the shell thickness to map the range that is safe to consider for the design of the hollow particle. Indeed, our results suggested that nanosized particles, whose core is $C < 200$ nm, demonstrated higher SOC, compared to microscaled particles. The predicted allowed dimensions for the shell indicate that a thinner core in the order of $C - B = 5$ nm would allow for SOC ≈ 0.77, which corresponds to almost fully lithiated Si ($Li_{3.75}Si$), and would therefore contribute to higher capacity of the half cell.

Summary. In summary, we performed ab initio simulations to predict the interface properties of equilibrated lithiated Si/C heterostructures and combined results from these simulations with analytical expressions from linear elastic fracture mechanics to study fracture and debonding of hollow Si/C core−shell particles. Our results suggest that upon lithiation the interface adhesion decreaases by only ∼20%, suggesting that the two active materials are not threatened by delamination, even at high stages of lithiation ($W_{sep} = 2.44$ J/m^2). The interfacial zone does not demonstrate segregation of Li, as it was for the lithiated Si/Cu interface, suggesting that Si termination is predominant on a C-surface, in agreement with our analysis in Supporting Information. Upon application of strain along the c-direction, the Si/C interface maintained its good adhesion and the heterostructure fractured within lithiated Si at 6.18 GPa with its fracture energy being more than five times (0.50 J/m^2) lower than the energy required to separate the interface (2.894 J/m^2). The calculated fracture and

dx.doi.org/10.1021/nl500410g | Nano Lett. XXXX, XXX, XXX−XXX

debonding parameters from the ab initio calculations were used as input parameters in linear elasticity analytical expressions to identify the optimum design conditions for the Si/C hollow core−shell structure. The constructed phase diagram outlined that high states of charge are achieved and failure is prevented if the thickness of the core is less than 200 nm and the thickness of the shell is approximately 5 nm.

■ ASSOCIATED CONTENT

Supporting Information

Systematic thermodynamics calculations of the surface stability criteria for various Li- and Si- nonstoichiometrically terminated diamond (111) surfaces and thorough electronic study of the bonding nature of the C-surface for the different terminations. This material is available free of charge via the Internet at http://pubs.acs.org.

■ AUTHOR INFORMATION

Corresponding Authors

*E-mail: (V.B.S.) vshenoy@seas.upenn.edu.
*E-mail: (M.E.S.) maria_stournara@brown.edu.
*E-mail: (Y.Q.) yueqi@egr.msu.edu.

Notes

The authors declare no competing financial interest.

■ ACKNOWLEDGMENTS

We gratefully acknowledge the support by the GM-Brown Collaborative Research Laboratory on Computational Materials Science and the GM computational resources. M.E.S. and Y.Q. also acknowledge the support from the Assistant Secretary for Energy Efficiency and Renewable Energy, Office of Vehicle Technologies of the U.S. Department of Energy (Contract No. DE-AC02-05CH11231, Subcontract No 7056410) under the Batteries for Advanced Transportation Technologies (BATT) Program. The authors declare no competing financial interest.

■ REFERENCES

(1) Beaulieu, L. Y.; Ebermanb, K. W.; Turnerb, R. L.; Krauseb, L. J.; Dahna, J. R. Colossal reversible volume changes in lithium alloys. *Electrochem. Solid-State Lett.* **2001**, *4* (9), A137−A140.

(2) Besenhard, J. O.; Yang, J.; Winter, M. Will advanced lithium-alloy anodes have a chance in lithium-ion batteries? *J. Power Sources* **1997**, *68* (1), 87−90.

(3) Hatchard, T. D.; Dahn, J. R In situ XRD and electrochemical study of the reaction *of lithium with amorphous silicon*. *J. Electrochem. Soc.* **2004**, *151* (6), A838−A842.

(4) Maranchi, J. P.; Hepp, A. F.; Evans, A. G.; Nuhfer, N. T.; Kumta, P. N. Interfacial properties of the a-Si/Cu: active-inactive thin-film anode system for lithium-ion batteries. *J. Electrochem. Soc.* **2006**, *153* (6), A1246−A1253.

(5) Wu, H.; Cui, Y. Designing nanostructured Si anodes for high energy lithium ion batteries. *Nano Today* **2012**, *7* (5), 414−429.

(6) Liu, N.; Wu, H.; McDowell, M. T.; Yao, Y.; Wang, C.; Cui, Y. A Yolk-Shell Design for Stabilized and Scalable Li-Ion Battery Alloy Anodes. *Nano Lett.* **2012**, *12* (6), 3315−3321.

(7) Deshpande, R.; Cheng, Y. T.; Verbrugge, M. W. Modeling diffusion-induced stress in nanowire electrode structures. *J. Power Sources* **2010**, *195* (15), 5081−5088.

(8) Verbrugge, M. W.; Cheng, Y. T. Stress and Strain-Energy Distributions within Diffusion-Controlled Insertion-Electrode Particles Subjected to Periodic Potential Excitations. *J. Electrochem. Soc.* **2009**, *156* (11), A927−A937.

(9) Chan, C. K.; Peng, H.; Liu, G.; McIlwrath, K.; Zhang, X. F.; Huggins, R. A.; Cui, Y. High-performance lithium battery anodes using silicon nanowires. *Nat. Nanotechnol.* **2008**, *3* (1), 31−35.

(10) Cheng, Y.-T.; Verbrugge, M. W. The influence of surface mechanics on diffusion induced stresses within spherical nanoparticles. *J. Appl. Phys.* **2008**, *104* (8), 083521.

(11) Magasinski, A.; Dixon, P.; Hertzberg, B.; Kvit, A.; Ayala, J.; Yushin, G. High-performance lithium-ion anodes using a hierarchical bottom-up approach. *Nat. Mater.* **2010**, *9* (4), 353−358.

(12) Park, M.-H.; Kim, M. G.; Joo, J.; Kim, K.; Kim, J.; Ahn, S.; Cui, Y.; Cho, J. Silicon Nanotube Battery Anodes. *Nano Lett.* **2009**, *9* (11), 3844−3847.

(13) Liu, X. H.; Zhong, L.; Huang, S.; Mao, S. X.; Zhu, T.; Huang, J. Y. Size-Dependent Fracture of Silicon Nanoparticles During Lithiation. *ACS Nano* **2012**, *6* (2), 1522−1531.

(14) Chen, Z. H.; Christensen, L.; Dahn, J. R. A study of the mechanical and electrical properties of a polymer/carbon black binder system used in battery electrodes. *J. Appl. Polym. Sci.* **2003**, *90* (7), 1891−1899.

(15) Christensen, J. Modeling Diffusion-Induced Stress in Li-Ion Cells with Porous Electrodes. *J. Electrochem. Soc.* **2010**, *157* (3), A366−A380.

(16) Li, H.; Huanga, X.; Chena, L.; Wub, Z.; Liangb, Y. A high capacity nano-Si composite anode material for lithium rechargeable batteries. *Electrochem. Solid-State Lett.* **1999**, *2* (11), 547−549.

(17) Sun, C. F.; Karki, K.; Jia, Z.; Liao, H.; Zhang, Y.; Li, T.; Qi, Y.; Cumings, J.; Rubloff, G. W.; Wang, Y. H. A Beaded-String Silicon Anode. *ACS Nano* **2013**, *7* (3), 2717−2724.

(18) Liu, G.; Xun, S.; Vukmirovic, N.; Song, X.; Velasco, P. O.; Zheng, H.; Battaglia, V. S.; Wang, L.; Yang, W. Polymers with Tailored Electronic Structure for High Capacity Lithium Battery Electrodes. *Adv. Mater.* **2011**, *23* (40), 4679−+.

(19) Wu, H.; Zheng, G.; Liu, N.; Carney, T. J.; Yang, Y.; Cui, Y. Engineering Empty Space between Si Nanoparticles for Lithium-Ion Battery Anodes. *Nano Lett.* **2012**, *12* (2), 04−909.

(20) Xu, Y. H.; Yin, G.; Ma, Y.; Zuo, P.; Cheng, X. Nanosized core/shell silicon@carbon anode material for lithium ion batteries with polyvinylidene fluoride as carbon source. *J. Mater. Chem.* **2010**, *20* (16), 3216−3220.

(21) Yao, Y.; McDowell, M. T.; Ryu, I.; Wu, H.; Liu, N.; Hu, L.; Nix, W. D.; Cui, Y. Interconnected Silicon Hollow Nanospheres for Lithium-Ion Battery Anodes with Long Cycle Life. *Nano Lett.* **2011**, *11* (7), 2949−2954.

(22) Shenoy, V. B.; Johari, P.; Qi, Y. Elastic softening of amorphous and crystalline Li-Si Phases with increasing Li concentration: A first-principles study. *J. Power Sources* **2010**, *195* (19), 6825−6830.

(23) Hertzberg, B.; Benson, J.; Yushin, G. Ex-situ depth-sensing indentation measurements of electrochemically produced Si-Li alloy films. *Electrochem. Commun.* **2011**, *13* (8), 818−821.

(24) Stournara, M. E.; Xiao, X.; Qi, Y.; Johari, P.; Lu, P.; Sheldon, B. W.; Gao, H.; Shenoy, V. B. Li Segregation Induces Structure and Strength Changes at the Amorphous Si/Cu Interface. *Nano Lett.* **2013**, *13* (10), 4759−4768.

(25) Kresse, G.; Furthmuller, J. Efficiency of ab-initio total energy calculations for metals and semiconductors using a plane-wave basis set. *Comput. Mater. Sci.* **1996**, *6* (1), 15−50.

(26) Kresse, G.; Furthmuller, J. Efficient iterative schemes for ab initio total-energy calculations using a plane-wave basis set. *Phys. Rev. B* **1996**, *54* (16), 11169−11186.

(27) Han, J. C.; Gao, W.; Zhu, J.; Meng, S.; Zheng, W. Density-functional theory study of the microstructure, electronic structure, and optical properties of amorphous carbon. *Phys. Rev. B* **2007**, *75* (15), 155418.

(28) McCulloch, D. G.; McKenzie, D. R.; Goringe, C. M. Ab initio simulations of the structure of amorphous carbon. *Phys. Rev. B* **2000**, *61* (3), 2349−2355.

(29) Endo, M.; Kim, C.; Nishimura, K.; Fujino, T.; Miyashita, K. Recent development of carbon materials for Li ion batteries.

(30) Kresse, G.; Joubert, D. From ultrasoft pseudopotentials to the projector augmented-wave method. *Phys. Rev. B* **1999**, *59* (3), 1758−1775.

(31) Perdew, J. P.; Burke, K.; Ernzerhof, M. Generalized gradient approximation made simple. *Phys. Rev. Lett.* **1996**, *77* (18), 3865−3868.
(32) Feynman, R. P. Forces in molecules. *Phys. Rev.* **1939**, *56* (4), 340−343.
(33) Verbrugge, M. W.; Qi, Y.; Baker, D. R.; Cheng, Y. Diffusion induced stress within core shell structures and implications for robust electrode design and materials systems. Submitted for publication.
(34) Chevrier, V. L.; Zwanziger, J. W.; Dahn, J. R. First principles studies of silicon as a negative electrode material for lithium-ion batteries. *Can. J. Phys.* **2009**, *87* (6), 625−632.
(35) Aydinol, M. K.; Kohan, A. F.; Ceder, G. Ab initio study of lithium intercalation in metal oxides and metal dichalcogenides. *Phys. Rev. B* **1997**, *56* (3), 1354−1365.
(36) Chevrier, V. L.; Dahn, J. R. First Principles Model of Amorphous Silicon Lithiation. *J. Electrochem. Soc.* **2009**, *156* (6), A454−A458.
(37) Wang, C. S.; Zhang, X.; Appleby, J.; Chen, X.; Little, F. E. Self-discharge of secondary lithium-ion graphite anodes. *J. Power Sources* **2002**, *112* (1), 98−104.
(38) Zhang, S. S.; Ding, M. S.; Xu, K.; Allen, J.; Jow, T. R. Understanding solid electrolyte interface film formation on graphite electrodes. *Electrochem. Solid-State Lett.* **2001**, *4* (12), A206−A208.
(39) Nazri, G.-A.; Gianfranco, P. *Lithium Batteries: Science and Technology*; Springer: New York, 2009.
(40) Becke, A. D.; Edgecombe, K. E. A Simple Measure of Electron Localization in Atomic and Molecular-Systems. *J. Chem. Phys.* **1990**, *92* (9), 5397−5403.
(41) Henkelman, G.; Arnaldsson, A.; Jonsson, H. A fast and robust algorithm for Bader decomposition of charge density. *Comput. Mater. Sci.* **2006**, *36* (3), 354−360.
(42) Sen, F. G.; Qi, Y.; Alpas, A. T. Anchoring platinum on graphene using metallic adatoms: a first principles investigation. *J. Phys.: Condens. Matter* **2012**, *24* (22), 225003.
(43) Chou, C.-Y.; Hwang, G. S. Role of Interface in the Lithiation of Silicon-Graphene Composites: A First Principles Study. *J. Phys. Chem. C* **2013**, *117* (19), 9598−9604.
(44) Qi, Y.; Hector, L. G. Adhesion and adhesive transfer at aluminum/diamond interfaces: A first-principles study. *Phys. Rev. B* **2004**, *69* (23), 235401.
(45) Petersen, K. E. Silicon as a mechanical material. *Proc. IEEE* **1982**, *70* (5), 420−456.
(46) Erickson, F.; Schweitz, J. A. Micromechanical fracture strength of silicon. *J. Appl. Phys.* **1990**, *68*, 5840.
(47) Field, J. E. The mechanical and strength properties of diamond. *Rep. Prog. Phys.* **2012**, *75* (12), 126505.
(48) Zhao, K. J.; Pharr, M.; Hartle, L.; Vlassak, J. J.; Suo, Z. Fracture and debonding in lithium-ion batteries with electrodes of hollow core-shell nanostructures. *J. Power Sources* **2012**, *218*, 6−14.
(49) Sethuraman, V. A.; Chon, M. J.; Shimshak, M.; Srinivasan, V.; Guduru, P. R. In situ measurements of stress evolution in silicon thin films during electrochemical lithiation and delithiation. *J. Power Sources* **2010**, *195* (15), 5062−5066.
(50) *Synthetic Diamond - Emerging CVD Science and Technology*; Spear, K. E., Dismukes, J. P., Eds.; Wiley: New York, 1994.

dx.doi.org/10.1021/nl500410g | *Nano Lett.* XXXX, XXX, XXX−XXX